JACS
JOURNAL OF THE AMERICAN CHEMICAL SOCIETY
pubs.acs.org/JACS
Article

Metal–Organic Phase-Change Materials for Thermal Energy Storage

Ryan D. McGillicuddy, Surendra Thapa, Malia B. Wenny, Miguel I. Gonzalez, and Jarad A. Mason*

Cite This: https://dx.doi.org/10.1021/jacs.0c08777
Read Online
ACCESS | Metrics & More | Article Recommendations | Supporting Information

ABSTRACT: The development of materials that reversibly store high densities of thermal energy is critical to the more efficient and sustainable utilization of energy. Herein, we investigate metal–organic compounds as a new class of solid–liquid phase-change materials (PCMs) for thermal energy storage. Specifically, we show that isostructural series of divalent metal amide complexes featuring extended hydrogen bond networks can undergo tunable, high-enthalpy melting transitions over a wide temperature range. Moreover, these coordination compounds provide a powerful platform to explore the specific factors that contribute to the energy density and entropy of metal–organic PCMs. Through a systematic analysis of the structural and thermochemical properties of these compounds, we investigated the influence of coordination bonds, hydrogen-bond networks, neutral organic ligands, and outer-sphere anions on their phase-change thermodynamics. In particular, we identify the importance of high densities of coordination bonds and hydrogen bonds to achieving a high PCM energy density, and we show how metal-dependent changes to the local coordination environment during melting impact the entropy and enthalpy of metal–organic PCMs. These results highlight the potential of manipulating order–disorder phase transitions in metal–organic materials for thermal energy storage.

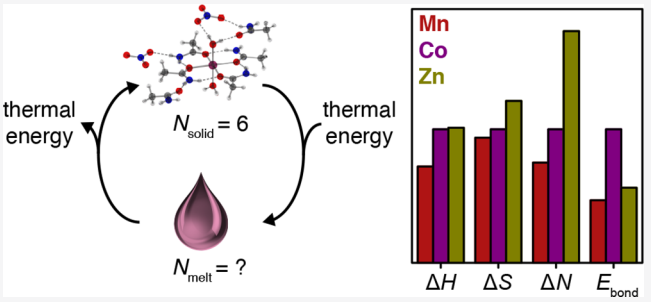

INTRODUCTION

With more than 90% of domestic energy production involving the generation of thermal energy and 60% of all generated energy wasted as heat,[1] mismatches between the time, place, and rate at which heat is generated and used—or dissipated—present myriad opportunities for improvements in performance and efficiency through the reversible storage of thermal energy.[2] Thermal energy storage materials are needed across a broad temperature range to, for instance, reduce the energy required to heat and cool buildings (25–150 °C),[3,4] optimize the efficiency of thermoelectrics (25–650 °C),[5,6] dissipate heat in electronics and data centers (30–80 °C),[7,8] increase the driving range of electric vehicles in cold climates (30–60 °C),[9] recover waste heat from industrial processes (40–1000 °C),[10] reduce emissions from combustion vehicle cold starts (250–350 °C),[11,12] and store solar energy (250–1000 °C).[13] Despite the tremendous importance of managing heat efficiently, the development of new thermal energy storage materials has received significantly less attention than materials for electrical and chemical energy storage,[2] particularly within the synthetic chemistry community.[14−17]

Although there are many ways to store thermal energy, the latent heat of an isothermal phase transition offers the potential for high energy densities without the large temperature swings that are the basis of sensible heat storage or the large volume and temperature changes that accompany thermochemical storage (Figure 1a).[18−21] In principle, any type of reversible, thermally induced phase transition can be used to store thermal energy, but phase-change materials (PCMs) that undergo solid–liquid transitions are the most promising for many applications. These transitions have higher latent heats than solid–solid transitions while avoiding the large volume changes that occur during solid–gas or liquid–gas transitions.[22] Though not often termed such, ice is one of the most recognizable and widely used solid–liquid PCMs for cold storage. Interest in the development of higher-temperature PCMs for thermal management above 0 °C began in the 1940s to improve the efficiency of heating and cooling in homes and advanced rapidly in the 1960s when NASA investigated a range of PCMs to regulate the temperature of sensitive electronic components and biological samples in outer space.[23,24] These early efforts relied almost exclusively on paraffins, which undergo sharp, reversible melting transitions with minimal hysteresis but relatively low volumetric energy densities,[25] and metal-salt hydrates, which undergo phase transitions with much higher energy densities but often have issues upon cycling due to phase separation, supercooling, and corrosivity.[19,26]

Received: August 14, 2020

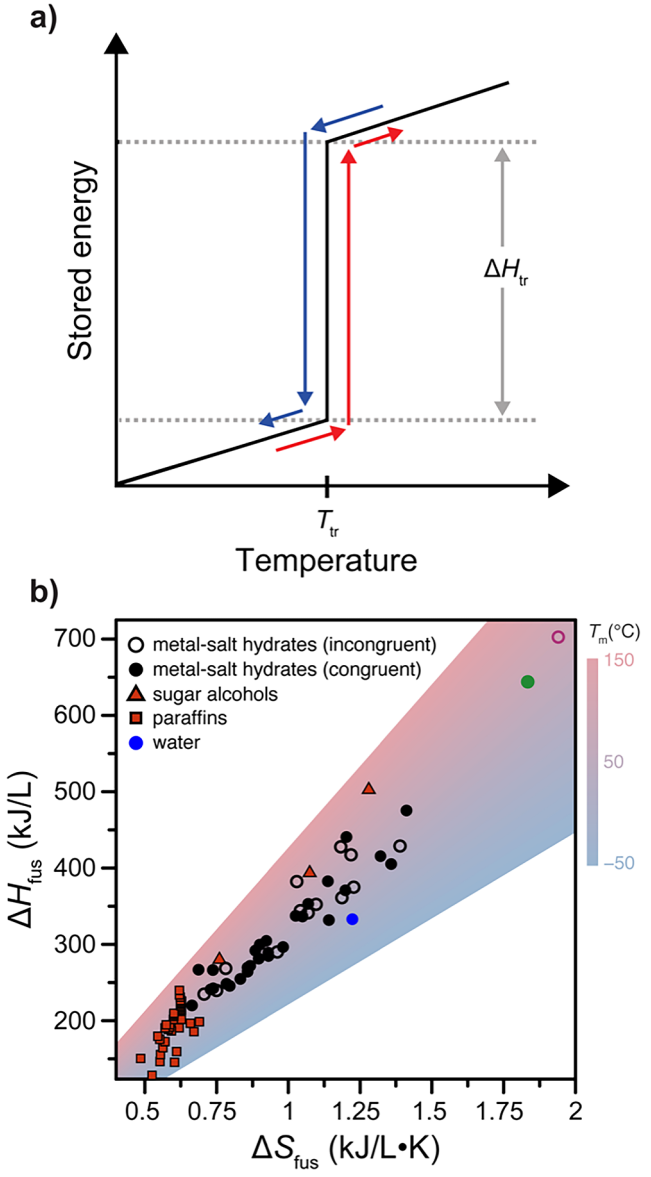

Figure 1. (a) Schematic illustrating a typical thermal energy storage cycle for a phase-change material (PCM). (b) Comparison of enthalpies of fusion, ΔH_{fus}, entropies of fusion, ΔS_{fus}, and melting temperatures, T_m, for conventional organic and inorganic PCMs. Green and purple symbols correspond to $Ba(OH)_2{\cdot}8H_2O$ and $Sr(OH)_2{\cdot}8H_2O$, respectively. Note that volumetric energy densities are calculated from gravimetric values using crystallographic densities.

The development of PCMs has continued to focus on simple inorganic and organic compounds, frequently relying on external systems or internal additives to augment the properties of existing materials.[27−29] These efforts have led to the commercialization of a range of PCMs,[30] but their energy density and overall performance have not been sufficient to warrant their use in many thermal applications. Given that engineering solutions increase the mass, volume, cost, and complexity of thermal energy storage systems, there has been surprisingly little effort to synthesize and evaluate new PCMs that might offer intrinsically better properties.[14−16,31] In particular, although metal−salt hydrates have received substantial attention, structurally similar metal−organic materials have yet to be seriously explored in the context of thermal energy storage despite their diverse range of modular and highly tunable structures. Unlike conventional organic and inorganic PCMs, the structure of metal−organic materials can be controlled through rational ligand design and directional coordination bonds to tailor the dimensionality, entropy, and strength of covalent and noncovalent interactions within a solid in a predictable fashion.[32,33] Beyond the potential implications for improved performance, tunable metal−organic PCMs offer a platform to establish fundamental structure−property relationships that provide insight into the thermodynamics and kinetics of phase transitions relevant to thermal energy storage.

The design of new solid−liquid PCMs requires controlling the enthalpy and entropy of both crystalline solid and disordered liquid phases, as the temperature of a first-order phase transition, T_{tr}, is dictated by the ratio of the enthalpy, ΔH_{tr}, and entropy, ΔS_{tr}, changes between the two phases with $T_{tr} = \Delta H_{tr}/\Delta S_{tr}$. As such, a high-energy (enthalpy) melting transition must be accompanied by a large entropy increase to occur at a moderate temperature. Owing, in part, to substantial variability in reported thermodynamic data—especially for inorganic compounds (Figure S2)—it is challenging to establish rigorous structure−property relationships for many classes of conventional PCMs.[16,34−36] Nonetheless, the high volumetric energy densities of select metal−salt hydrates offer inspiration for the design of metal−organic PCMs. In particular, two metal−salt hydrates, $Ba(OH)_2{\cdot}8H_2O$ and $Sr(OH)_2{\cdot}8H_2O$, undergo melting transitions with exceptionally high enthalpies of fusion, ΔH_{fus}, of 644 kJ/L at 78 °C and 703 kJ/L at 89 °C,[37,38] respectively (Figure 1b), the latter of which is more than double the energy density of ice (333 kJ/L) and approaching the energy density of a 9 V battery (782 kJ/L).[39]

Both $Ba(OH)_2{\cdot}8H_2O$ and $Sr(OH)_2{\cdot}8H_2O$ have similar solid-state structures, wherein eight coordinated H_2O molecules and two outer-sphere hydroxide anions per metal cation interact through a dense network of intermolecular hydrogen bonds.[40,41] Although the exact structural and chemical features responsible for their high energy densities are not well understood, differences between the strength and density of hydrogen bonds within each solid and liquid phase likely play an important role.[16] Indeed, many sugar alcohols also feature dense hydrogen bond networks and have relatively large volumetric enthalpies of fusion,[42] albeit with a propensity to degrade above their melting temperatures.[43] Similarly, both $Ba(OH)_2{\cdot}8H_2O$ and $Sr(OH)_2{\cdot}8H_2O$ are subject to poor cyclability because of phase separation and supercooling.[44,45] An improved understanding of how hydrogen-bonding networks can be manipulated to tune the thermodynamics of order−disorder phase transitions could dramatically expand the library of candidate high-enthalpy PCMs.[46]

Herein, we report an initial study of metal−organic compounds as PCMs for thermal energy storage. Specifically, we synthesized isostructural series of simple coordination compounds with extended hydrogen-bond networks similar to those found in metal−salt hydrates and investigated the influence of the structure and composition of these compounds on their enthalpies and entropies of fusion. To achieve high densities of hydrogen bonds and moderate (<200 °C) melting temperatures, we selected small organic molecules, including methylurea (MeUr) and acetamide ($AcNH_2$), that feature multiple hydrogen bond donor and acceptor groups and are known to form weak coordination bonds with metal cations as neutral ligands.[47] Although many coordination complexes of small amides have been crystallographically characterized, the

https://dx.doi.org/10.1021/jacs.0c08777
J. Am. Chem. Soc. XXXX, XXX, XXX−XXX

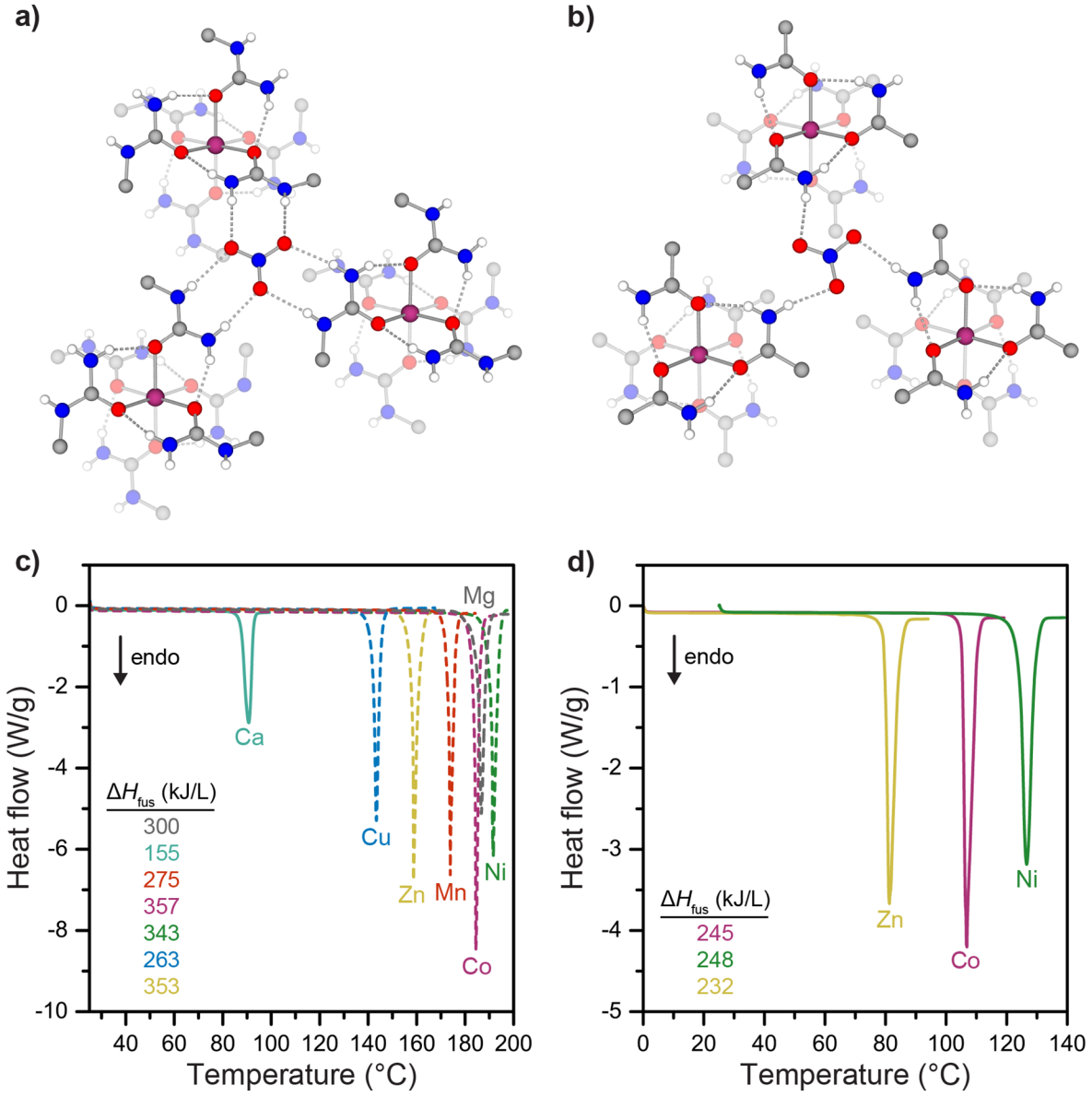

Figure 2. Crystal structures of (a) $[Co(MeUr)_6](NO_3)_2$ and (b) $[Co(AcNH_2)_6](NO_3)_2$. Gray, red, blue, white, and purple spheres represent C, O, N, H, and Co atoms, respectively. H atoms not bound to N atoms are omitted for clarity, and dashed lines indicate intramolecular and intermolecular hydrogen bonds. Differential scanning calorimetry (DSC) traces for (c) $[M(MeUr)_6](NO_3)_2$ and (d) $[M(AcNH_2)_6](NO_3)_2$ compounds. Solid lines indicate that the transition is reversible upon cooling, while dashed lines indicate irreversible transitions.

thermodynamic data required to evaluate their potential as PCMs have rarely been measured, and there is limited understanding of the structural and chemical factors that govern their melting thermodynamics.

RESULTS AND DISCUSSION

With its propensity to form dense hydrogen bond networks, urea represents a particularly promising ligand for metal–organic PCMs,[48] but rapid decomposition within melts effectively rules out its usefulness for reversible thermal energy storage.[49,50] To target high hydrogen bond densities without decomposition or undesirable reactivity in the liquid phase, we thus began by exploring coordination complexes of *N*-methylurea (MeUr), where the addition of a methyl group trades one hydrogen bond donor for substantially improved thermal stability. When combined with divalent metal halide or nitrate salts, MeUr forms a series of octahedral complexes $[M(MeUr)_6]X_2$ (M = Mg, Ca, Mn, Co, Ni, Cu, Zn; X = Cl or NO_3).[47a,b] Within these compounds, octahedral metal centers direct the formation of intramolecular hydrogen bonds between the metal-bound carbonyl O atoms and the N–H groups on adjacent MeUr ligands and of extended networks of intermolecular hydrogen bonds between MeUr ligands and uncoordinated anions (Figure 2a and Figure S6, Tables S4–S7).

To evaluate the effectiveness of MeUr as a ligand for metal–organic PCMs—as well as how the choice of metal cation and outer-sphere anion affects PCM energy density—differential scanning calorimetry (DSC) was used to determine ΔH_{fus}, ΔS_{fus}, and T_m for these materials. Although all $[M(MeUr)_6]Cl_2$ compounds melted prior to decomposition, $[Mn(MeUr)_6]Cl_2$ was the only analogue to exhibit a reversible melting transition (Figure S5), with ΔH_{fus} of 194 kJ/L and ΔS_{fus} of 0.50 kJ L^{-1} K^{-1} at 115.8 °C—values that are lower than many metal–salt

https://dx.doi.org/10.1021/jacs.0c08777
J. Am. Chem. Soc. XXXX, XXX, XXX–XXX

hydrate and sugar alcohol PCMs around this temperature (Figure 1b). Note that thermodynamic values are often reported on a molar basis, but mass and volume are far more relevant to energy storage applications. Since available space is often a limiting factor, maximizing the energy density of a PCM requires maximizing enthalpy changes on a volumetric basis. Here, volumetric quantities are calculated from measured gravimetric values using crystallographic densities to facilitate comparisons between the intrinsic properties of different materials.[51]

Replacing Cl with NO_3 yields the structurally similar compound $[Mn(MeUr)_6](NO_3)_2$, which melts with a much higher ΔH_{fus} of 275 kJ/L and ΔS_{fus} of 0.62 kJ L^{-1} K^{-1} at 173 °C (Figure 2c). Both Mn compounds have a similar density of intra- and intermolecular hydrogen bonds, but the size and shape of the NO_3 anion better match the pocket of amide donor groups surrounding it, enabling the formation of closer and more linear donor−acceptor interactions than are possible with Cl (Tables S4 and S6).[16,52] In addition, although Cl anions typically form stronger hydrogen bonds to a single donor,[53] the acceptor strength of Cl likely falls off more quickly than that of NO_3 as the number of hydrogen bonds increases. While other hydrogen bond acceptors are also of interest, the initial metal−organic PCMs explored here thus contain NO_3 anions.

Melting transitions across the series of isostructural $[M(MeUr)_6](NO_3)_2$ compounds occur between 89 and 191 °C, with ΔH_{fus} ranging from 155 kJ/L for the Ca analogue to 357 kJ/L for the Co analogue (Figure 2a,c). All melting transitions are irreversible with the exception of the Ca analogue, which is the only compound in the series that melts below 100 °C. Although the DSC traces for these compounds do not show any extra heat signals corresponding to decomposition, NMR spectra of dissolved $[Zn(MeUr)_6](NO_3)_2$ after melting indicate a small amount of MeUr decomposition—likely due to the formation of methylammonium and cyanate—which may be sufficient to inhibit recrystallization (Figure S7).[54] Any partial decomposition, however, is unlikely to impact melting thermodynamics as the DSC heat flow curves quickly return to baseline after melting (Figure 2c). As such, the thermophysical properties of these materials can be compared to gain insight into the relative importance of the metal in modulating melting behavior.

The energy density of the $M(MeUr)_6(NO_3)_2$ series of compounds is highly dependent on the identity of the metal cation with Ca < Cu < Mn < Mg < Ni < Zn ≈ Co, which—aside from Cu and Ni—is roughly consistent with the expected trend of increasing M−MeUr bond strengths.[55] Stronger M−MeUr bonds could contribute to higher ΔH_{fus} through two primary mechanisms: (1) directly because of a decrease in metal coordination number during melting and (2) indirectly by modulating hydrogen bond strength either through polarization of MeUr ligands that strengthens intra- and intermolecular hydrogen bonds via inductive effects or through shorter M−MeUr bonds that decrease the distance between intramolecular hydrogen bond donors and acceptors. The relative contribution of each of these effects depends, in part, on the magnitude of changes to the average metal coordination number and the density of hydrogen bonds upon transitioning from the solid to liquid state.

The crystal structures of $[M(MeUr)_6](NO_3)_2$ offer additional insight into how metal−ligand and hydrogen-bonding interactions impact the metal dependency of ΔH_{fus}. For instance, the Cu and Co analogues have the same average coordination bond distance (M−O = 2.1002(15) and 2.0980(14) Å, respectively), average intramolecular donor−acceptor hydrogen bond distance (N···O = 2.853(3) and 2.857(3) Å, respectively), and average intermolecular hydrogen bond distances (N···O = 2.986(3) and 2.980(3) Å, respectively), but the transition enthalpy of Cu (263 kJ/L) is 26% lower than that of Co (357 kJ/L). Although average distances are identical, a Jahn−Teller distortion in the Cu complex leads to pairs of long (2.2187(17) Å) and short (1.977(1) Å) metal−ligand bonds and, consequently, pairs of long (2.950(3) Å) and short (2.7757(17) Å) intramolecular hydrogen bonds, while all hydrogen bonds in the Co compound are, as expected, of more uniform length (Tables S6 and S7). If both compounds experience a similar partial loss of coordination bonds and hydrogen bonds upon conversion to a liquid, then the presence of weaker sets of intramolecular bonds in $[Cu(MeUr)_6](NO_3)_2$ could be responsible for its lower transition enthalpy.

The important contribution of intramolecular interactions to PCM thermodynamics is further emphasized by the low transition enthalpy of the Ca analogue (155 kJ/L). In this compound, the large ionic radius of Ca leads to longer intramolecular hydrogen bonds (average N···O distance = 3.0122(17) Å) but similar intermolecular hydrogen bond distances (Tables S6 and S7), suggesting that intramolecular interactions contribute more than intermolecular interactions to energy density differences between metals and that strong intramolecular interactions are needed to achieve a high phase-change energy density in this class of coordination compounds. In addition to impacting enthalpy, the weaker intramolecular interactions in $[Ca(MeUr)_6](NO_3)_2$ also likely increase the solid-state residual motion of MeUr, thus increasing the vibrational and rotational entropy within the solid and decreasing ΔS_{fus} (0.43 and 0.78 kJ L^{-1} K^{-1} for the Ca and Co analogues, respectively) as less entropy will be created upon melting.[56] The decrease in entropy does not, however, compensate for the proportionally larger loss in enthalpy, leading to a 95.0 °C lower melting temperature.

To promote reversibility and further explore structure−property relationships, we next targeted metal−organic PCMs with acetamide ($AcNH_2$) ligands, which are more thermally stable than Ur and MeUr but still have closely spaced hydrogen bond donor and acceptor groups.[47c] Eutectic mixtures of acetamide and a few metal nitrates have been evaluated as PCMs for thermal energy storage,[57] but to the best of our knowledge, the phase-change thermodynamics of metal−acetamide compounds—with well-defined, uniform structures—have not been studied. It is also worth noting that eutectic melting transitions are inherently incongruent, which can present issues for long-term performance upon repeated cycling, particularly if any supercooling occurs.[58]

Though structurally similar to $[M(MeUr)_6](NO_3)_2$, $[M(AcNH_2)_6](NO_3)_2$ (M = Co, Ni, Zn) compounds exhibit very different thermal behavior, with melting transitions that are nearly 80 °C lower in temperature and more than 100 kJ/L lower in enthalpy than their MeUr congeners (Figure 2b,d). These differences can be attributed to changes in the hydrogen-bond networks present within each series of compounds. Even though intramolecular hydrogen-bonding interactions are similar—with close to 10 and 8 intramolecular hydrogen bonds per nm^3 for $[M(AcNH_2)_6](NO_3)_2$ and $[M(MeUr)_6](NO_3)_2$, respectively—the $AcNH_2$ complexes

https://dx.doi.org/10.1021/jacs.0c08777
J. Am. Chem. Soc. XXXX, XXX, XXX−XXX

have a much lower density of intermolecular hydrogen bonds (~10 per nm^3) than the MeUr compounds (~16 per nm^3) due to the loss of a hydrogen bond donor group (Table S3).

In addition to a lower melting enthalpy, DSC revealed that $[M(AcNH_2)_6](NO_3)_2$ melting transitions were reversible but alternated between two distinct melting temperatures upon cycling (Figure S21). Through a combination of powder and single-crystal X-ray diffraction experiments, the two melting transitions were found to originate from trigonal or cubic phases of each compound, with the cubic phases melting at a higher temperature (Figures S18 and S19). These different phases arise from changes to the relative orientation of NO_3 anions that alter the long-range structure of hydrogen bond networks within each material. While multiple meltable phases might complicate the controllable release of thermal energy, such behavior offers an opportunity to manipulate the storage temperature in response to changing demands,[15,59] provided that the switching between phases could be controlled in a predictable fashion.

While synthesizing $[M(AcNH_2)_6](NO_3)_2$, we noticed that the presence of H_2O during crystallization led exclusively to the formation of the isostructural series of compounds $[M(AcNH_2)_4(H_2O)_2](NO_3)_2{\cdot}2AcNH_2$ (**1**-M, M = Mg, Mn, Fe, Co, Ni, Cu, Zn) under a wide range of conditions.[60] These compounds contain octahedral metal centers with four equatorial $AcNH_2$ ligands and two axial H_2O ligands, along with two uncoordinated $AcNH_2$ molecules per metal center. The partial displacement of bound $AcNH_2$ by H_2O leads to a much denser network of intermolecular hydrogen bonds (average of 18 per nm^3) than is present in $M(AcNH_2)_6(NO_3)_2$ (average of 10 per nm^3) (Table S3). This extended network consists of two-dimensional sheets of hydrogen bonds between NO_3 (acceptor), free $AcNH_2$ (donor/acceptor), and coordinated $AcNH_2$ (donor) that are linked in the third dimension by hydrogen bonds to coordinated H_2O (Figure 3a).

Excitingly, all **1**-M compounds undergo high-enthalpy, reversible melting transitions with ΔH_{fus} ranging from 276 to 327 kJ/L, values that are much higher than $[M(AcNH_2)_6](NO_3)_2$ and comparable to $[M(MeUr)_6](NO_3)_2$ and many metal−salt hydrates (Figure 3b). Moreover, a substantial increase in ΔS_{fus} (Table S1) leads to melting temperatures as much as 92 °C lower than the MeUr compounds and, consequently, fully reversible transitions for all members of the **1**-M series except **1**-Fe, for which oxidation of Fe(II) by NO_3 after melting precludes its use as a PCM. Similar to $[M(MeUr)_6](NO_3)_2$, the energy density of all **1**-M compounds except **1**-Cu and **1**-Ni roughly follow the Irving−Williams stability order—increasing in ΔH_{fus} with increasing M−L bond stability (Table S1).

To begin to unravel the factors that contribute to the metal dependency of **1**-M energy density, we used infrared spectroscopy (IR) and X-ray crystallography to directly probe hydrogen bond strength in the solid state (Figure 4a). The N−H stretching mode of primary amides occurs near 3460 cm^{-1} in the absence of hydrogen bonding.[61] Upon formation of a hydrogen bond to the carbonyl of another amide, this band red-shifts and broadens, with larger red-shifts indicative of stronger hydrogen bonds.[62] In the ambient temperature IR spectra of **1**-M, we observe weak bands centered from 3338 to 3300 cm^{-1} depending on the identity of the metal, with compounds that undergo higher enthalpy melting transitions exhibiting increasingly red-shifted stretching frequencies and shorter intramolecular hydrogen bonds

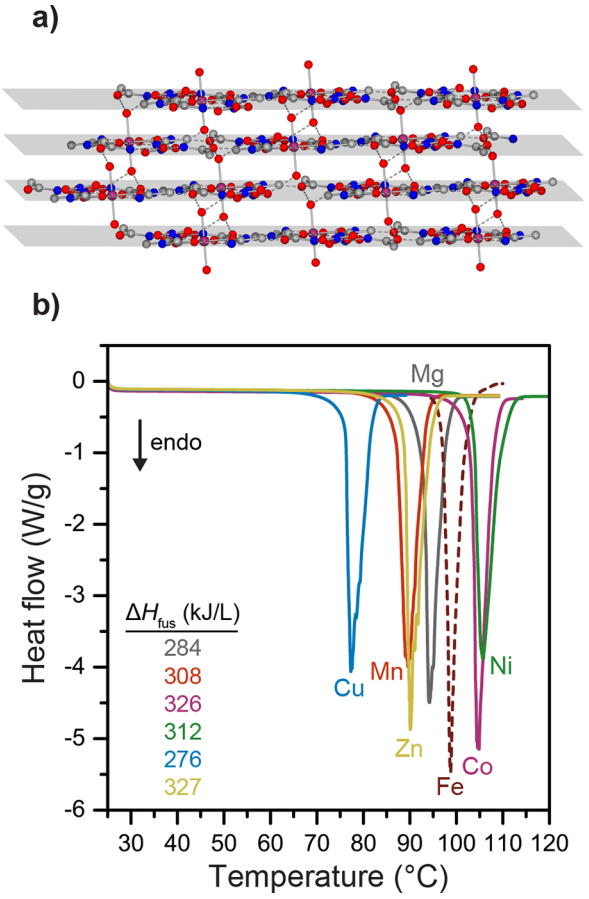

Figure 3. (a) Crystal structure of **1**-Co, with two-dimensional sheets of hydrogen bonds indicated by gray {$\bar{1}$12} planes. Gray, red, blue, and purple spheres represent C, O, N, and Co atoms, respectively. H atoms are omitted for clarity, and dashed lines indicate intramolecular and intermolecular hydrogen bonds. (b) DSC traces for isostructural **1**-M compounds. Solid lines indicate that the transition is reversible upon cooling, while a dashed line indicates an irreversible transition.

between bound $AcNH_2$ ligands (Figure 4b,c and Figure S29). In addition, all bands are red-shifted compared to that of $[Co(AcNH_2)_6](NO_3)_2$, which has 0.1 Å longer intramolecular hydrogen bonds than **1**-Co and a lower phase-change enthalpy than any **1**-M analogue. Because the total energy of intramolecular hydrogen bonds between four amides should exceed 100 kJ/mol,[63] changes to hydrogen-bonding strength should be of the correct magnitude to be a significant driver of differences in ΔH_{fus}, which span 21 kJ/mol, across the **1**-M series.

The preceding crystallographic and IR data highlight correlations between intramolecular hydrogen bond strength—as mediated by ligand sterics and the size and charge density of the central metal cation—and PCM energy density. However, these results provide an incomplete picture of phase-change thermodynamics as they only concern interactions within the solid state, and it is the difference between interactions within the solid and liquid phases that ultimately determines energy density. Stated differently, stronger interactions within an ordered phase will only lead to a higher energy density for a PCM if a sufficient fraction of those interactions are broken upon conversion to a more disordered phase. Moreover, while differences in metal−ligand and hydrogen bond strength can help rationalize enthalpic

https://dx.doi.org/10.1021/jacs.0c08777
J. Am. Chem. Soc. XXXX, XXX, XXX−XXX

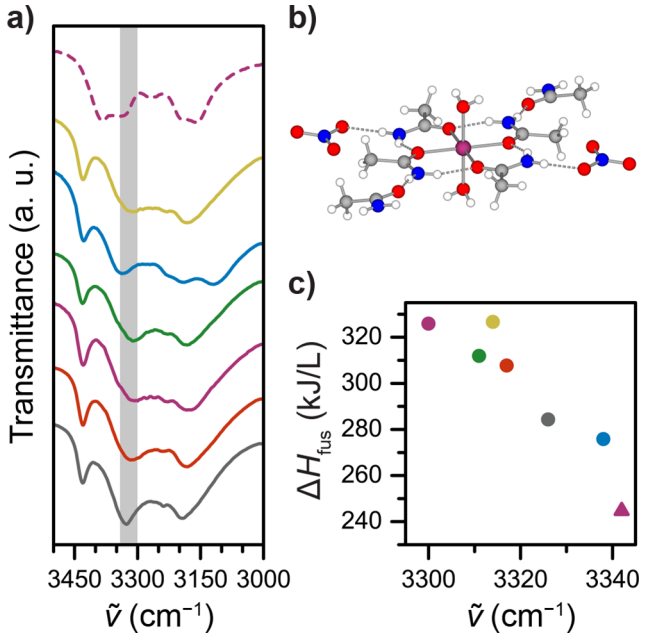

Figure 4. (a) Infrared spectra of **1**-M at ambient temperature for M = Mg (gray), Mn (red), Co (purple), Ni (green), Cu (blue), and Zn (yellow). The infrared spectrum of $[Co(AcNH_2)_6](NO_3)_2$ is also shown as a dashed purple line. (b) Intramolecular hydrogen bonds of **1**-Co are depicted with dashed lines. Gray, red, blue, white, and purple spheres represent C, O, N, H, and Co atoms, respectively. (c) N−H stretching frequency highlighted in (a) is inversely correlated to ΔH_{fus} in **1**-M (circles) and $[Co(AcNH_2)_6](NO_3)_2$ (triangle).

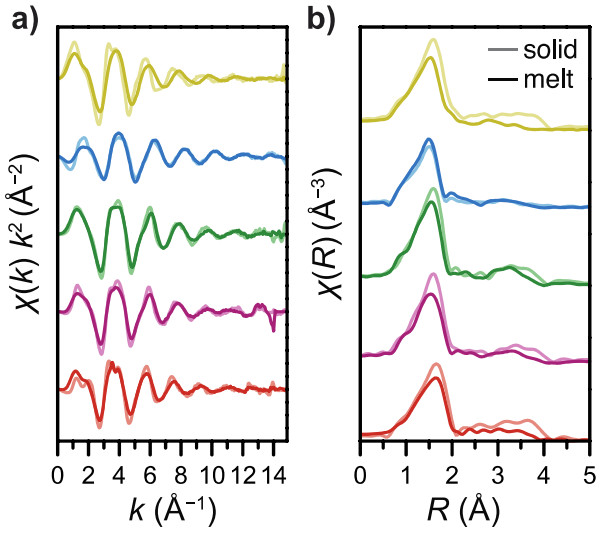

Figure 5. (a) Variable temperature EXAFS spectra of **1**-M at ambient temperature (lighter traces) and above the melting temperature (darker traces) for M = Mn (red), Co (purple), Ni (green), Cu (blue), and Zn (yellow). (b) Fourier transforms of the *k*-space EXAFS spectra at ambient temperature (lighter traces) and above the melting temperature (darker traces).

trends across the **1**-M series, solid-state characterization offers limited insight into entropic differences, and consequently, transition temperatures. For instance, **1**-Co and **1**-Zn have within error, the same ΔH_{fus}, but **1**-Zn has a 4% greater ΔS_{fus} that leads to a 15 °C lower melting temperature. With nearly identical crystal structures, rationalizing this entropy difference requires consideration of the structures of the liquids formed by each compound after melting.

To probe the average local structure of **1**-M in the liquid state, we used variable-temperature extended X-ray absorption fine structure (EXAFS) analysis to quantify changes during melting to coordination number and M−O distance within the first coordination sphere of analogues (M = Mn, Co, Ni, Cu, Zn) with easily accessible K-edge energies (Figure 5). EXAFS is routinely used to study the structure of liquids containing solvated metal salts at ambient temperature but, to the best of our knowledge, has rarely been applied to study the structure of metal−organic melts.[64,65] For each **1**-M compound, the first scattering shell—consisting of a pseudo-octahedral arrangement of oxygen atoms—was modeled at room temperature and just above the melting temperature. Absolute coordination numbers determined by modeling EXAFS data are typically subject to large errors because the absolute amplitude of scattering paths depends on many parameters, in addition to the coordination number, that are often highly correlated.[66] Here, the use of room temperature EXAFS data—for which scattering paths are already known from crystal structures—as a standard allowed for the more accurate determination of coordination numbers when compounds were melted *in situ*.

Although all **1**-M compounds are coordinatively saturated with six ligands in the solid state, EXAFS models revealed metal-dependent decreases in coordination number upon melting, with **1**-Zn undergoing the largest change to an average coordination number of 4.6(3). More modest decreases were observed for **1**-Mn and **1**-Co to average coordination numbers of 5.8(5) and 5.5(5), respectively, while **1**-Ni, which has the most stable metal−ligand bonds of the series,[55] remained coordinatively saturated with 6.1(5) ligands. As expected, M−O bond distances within the first coordination shell contracted the most for **1**-Zn, which had the largest decrease in coordination number (Table S18).

The substantial decrease in coordination number for **1**-Zn during melting is consistent with the lower coordination numbers that have been observed for solvated Zn^{2+} ions—relative to other first-row transition metal ions—in dimethylacetamide and tetramethylurea solutions at ambient temperature.[67] Moreover, these results provide direct structural insight into the liquid phase of each **1**-M analogue that help rationalize deviations of energy density trends from the Irving−Williams series. For instance, the low coordination number of molten Zn^{2+} ions is likely responsible for the large entropy difference between the solid and liquid phases of **1**-Zn—which has the highest ΔS_{fus} of the **1**-M series—because of the increased rotational, vibrational, and translational degrees of freedom that become accessible to dissociated ligands. This can explain why, as mentioned above, **1**-Zn has the same ΔH_{fus} as **1**-Co but a larger ΔS_{fus}. Specifically, the EXAFS models and thermodynamic data suggest that even though **1**-Zn may have weaker metal−ligand bonds than **1**-Co, the enthalpy change for dissociating a greater number of more weakly bound ligands in the former compound is roughly equivalent to dissociating a smaller number of more strongly bound ligands in the latter compound. This leads to similar energy densities for both PCMs but a larger entropic driving force—and, consequently, a lower melting temperature—for **1**-Zn. Following a similar logic, since **1**-Ni maintains a full coordination sphere after melting, it has a lower ΔH_{fus} than **1**-Co and **1**-Zn, even though **1**-Ni should have the strongest metal−ligand bonds. Note that one does not expect the full metal−ligand bond dissociation energy to be reflected in the

https://dx.doi.org/10.1021/jacs.0c08777
J. Am. Chem. Soc. XXXX, XXX, XXX−XXX

phase-transition enthalpy since new ligand−ligand interactions in the melt will partially compensate for broken coordination bonds and intramolecular hydrogen bonds.

Unlike **1**-M, the energy densities and melting temperatures of $[M(AcNH_2)_6](NO_3)_2$ increase with increasing metal−ligand bond strength (Zn < Co < Ni). Variable-temperature EXAFS spectra provide insight into why different trends are observed for the two series of compounds. In particular, EXAFS models of molten $[Co(AcNH_2)_6](NO_3)_2$ and $[Zn(AcNH_2)_6](NO_3)_2$ reveal average coordination numbers of 4.7(5) and 4.1(3), respectively, in each liquid phase. Both of these values are lower than those for molten **1**-M, which is attributable to the increased steric bulk around each metal center, but the relative decrease for the Co analogue is more substantial. In both $[M(AcNH_2)_6](NO_3)_2$ and **1**-M, the Co analogues have higher melting temperatures than the Zn compounds. However, the higher melting temperature of **1**-Co is due to a lower ΔS_{fus}, while that of $[Co(AcNH_2)_6](NO_3)_2$ is due mostly to a higher ΔH_{fus} (Figure 6). This is a direct result

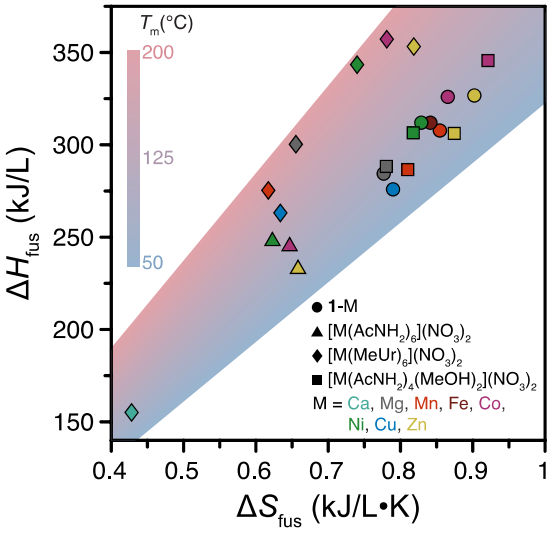

Figure 6. Comparison of ΔH_{fus}, ΔS_{fus}, and T_m for all metal−organic PCMs reported here. The symbol shape identifies the class of compounds, while the symbol color indicates the metal. Note that volumetric energy densities are calculated from gravimetric values using crystallographic densities.

of the different relative coordination number changes upon melting, whereby stronger Co−ligand bonds make a greater contribution to ΔH_{fus} in $[Co(AcNH_2)_6](NO_3)_2$.

The different liquid structures of metal−organic PCMs cause their phase-change thermodynamics to deviate from classical models of enthalpy−entropy compensation (Figure 6), which anticipate a linear, positive correlation between enthalpy and entropy changes in systems subject to the association and dissociation of weak interactions, such as those described here.[68,69] For instance, **1**-Mn and **1**-Zn have similar melting temperatures that are both below **1**-Co, but the lower melting temperature of **1**-Mn relative to **1**-Co is due primarily due to a decrease in ΔH_{fus}—owing to weaker metal−ligand and intramolecular hydrogen bonds—while that of **1**-Zn relative to **1**-Co is due to an increase in ΔS_{fus}—owing to a greater decrease in coordination number upon melting. As all three compounds are isostructural in the solid state, these results highlight the importance of understanding liquid—or disordered—structures in designing PCMs for thermal energy storage.

We note that the coordination environment of Cu^{2+} ions in weak oxygen-donor solvents has been the subject of some debate, with various models invoking square-planar, tetragonally elongated square-pyramidal, and centrosymmetric or noncentrosymmetric tetragonally elongated octahedral geometries, as well as dynamic equilibria between multiple geometries.[70] The EXAFS data for molten **1**-Cu indicate that Cu^{2+} ions maintain all four strongly bound equatorial ligands in the liquid phase, but as with previous solution studies at lower concentrations and temperatures, the state of more weakly bound axial ligands is subject to uncertainty. We found that a two-path model with four equatorial ligands and one axial ligand exhibited excellent agreement with experimental data, but the presence or absence of a second, perhaps more weakly bound,[70e] axial ligand could not be resolved. Although the EXAFS data do not allow the extent to which axial ligands remain bound in the liquid phase to be clearly determined, the low ΔH_{fus} and ΔS_{fus} of **1**-Cu are consistent with minimal changes to the coordination environment of Cu centers upon melting. In particular, the far weaker pair of metal−ligand and intramolecular hydrogen bonds in the solid state that arise from a Jahn−Teller distortion should lead to more weakly bound ligands that have greater residual motion in the solid state and, as a result, a smaller increase in vibrational and rotational entropy upon melting. Compared to other **1**-M compounds, the enthalpic effect of the Jahn−Teller distortion, however, is more substantial than entropic effects, leading to the lowest melting temperature of the series.

With a mixture of coordinated and uncoordinated Ac even in the solid state, we also wanted to understand the contribution of free Ac to the thermodynamics of **1**-M PCMs. To this end, we synthesized the compounds $[M(AcNH_2)_4(H_2O)_2](NO_3)_2$ (M = Mn, Co), which maintain the same coordination environment around each metal center but do not contain free $AcNH_2$.[47c] In the absence of free $AcNH_2$, the sheetlike hydrogen bond network of **1**-M is lost, and NO_3 anions twist away from the equatorial plane of $AcNH_2$ ligands to form hydrogen bonds to H_2O and $AcNH_2$ (Figure S24), leading to longer, weaker intermolecular hydrogen bonds indicative of a less stable extended structure (Tables S8 and S9). In fact, these compounds partially convert into **1**-M immediately upon melting as evidenced by powder X-ray diffraction and the presence of two overlapping endotherms in DSC traces (Figures S22 and S23), which prevents the extraction of any useful thermodynamic information.

As an alternative, we hypothesized that removing a single hydrogen bond donor from each axial ligand—by, for instance, replacing H_2O with methanol (MeOH)—would inhibit the formation of a compound with free Ac by reducing the enthalpic driving force for such a structure. As anticipated, the series of compounds $[M(AcNH_2)_4(MeOH)_2](NO_3)_2$ (M = Mg, Mn, Co, Ni, Cu, Zn) contain two-dimensional hydrogen bond networks similar to those in **1**-M and undergo reversible melting transitions (Figure 7). Moreover, ΔH_{fus} and ΔS_{fus} for these compounds are comparable to—and, in some cases, higher than—**1**-M despite their nearly 25% lower density of hydrogen bonds (Table S3). These similar enthalpies thus confirm the important contribution of changes to other types of interactions to the energy density of metal−organic PCMs and suggest that free $AcNH_2$ is not necessary to achieve a high energy density in acetamide-based PCMs. Indeed, [M-

https://dx.doi.org/10.1021/jacs.0c08777
J. Am. Chem. Soc. XXXX, XXX, XXX−XXX

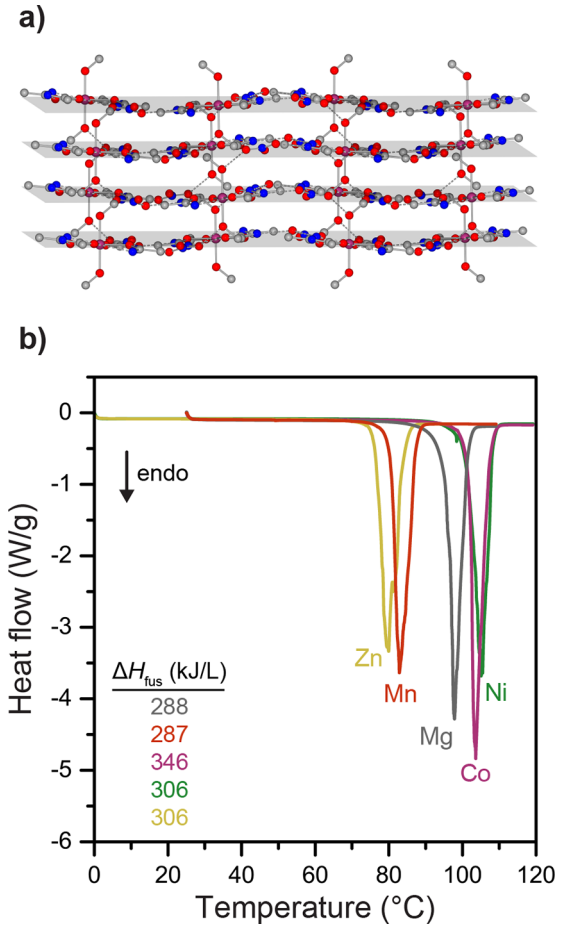

Figure 7. (a) Crystal structure of $[Co(AcNH_2)_4(MeOH)_2](NO_3)_2$, with two-dimensional sheets of hydrogen bonds indicated by gray {102} planes. Gray, red, blue, and purple spheres represent C, O, N, and Co atoms, respectively. H atoms are omitted for clarity, and dashed lines indicate intramolecular and intermolecular hydrogen bonds. (b) DSC traces for the isostructural series of $[M(AcNH_2)_4(MeOH)_2](NO_3)_2$ compounds.

$(AcNH_2)_4(MeOH)_2](NO_3)_2$ has a nearly 25% higher density of coordination bonds, on a volumetric basis, than **1**-M, likely offsetting the enthalpic impact of the decreased hydrogen bond density. In addition, $[M(AcNH_2)_4(MeOH)_2](NO_3)_2$ compounds have similar or higher volumetric—and gravimetric—energy densities compared to many metal−salt hydrates, despite their lower densities of hydrogen bonds.

Although this work has focused on the thermodynamics, rather than kinetics, of metal−organic PCMs, consideration of hysteresis—or supercooling—between melting and crystallization transitions is also important for many thermal energy storage applications.[71] Minimizing the degree of supercooling maximizes the amount of heat that can be stored and released over a narrow temperature range, while substantial supercooling leads to energy losses but offers the possibility of ambient temperature—uninsulated—storage coupled to the controlled release of heat through application of an external stimulus.[72] Among the reversible metal−organic PCMs studied here, the hysteresis observed in DSC experiments varies widely, with some compounds, such as and $[Ca(MeUr)_6](NO_3)_2$ and $[Mg(AcNH_2)_4(MeOH)_2](NO_3)_2$, exhibiting minimal supercooling and smaller energy losses on freezing (Table S2, Figures S20 and S26). Additionally, several compounds showed cold-crystallization behavior—crystallization during heating followed by melting—which can result from kinetically inhibited freezing. While understanding how to manipulate the kinetics of metal−organic PCMs will be of interest for future studies and for the design energy-efficient PCMs, we note that DSC measurements performed on milligram quantities of sample often show substantial supercooling that is lessened at larger scales[73] or upon the addition of small amounts of nucleating agents that do not significantly impact energy density.[74,75] In addition to crystallization kinetics, studying the corrosivity of metal−organic PCMs will also be important for evaluating their thermal energy storage potential.[76]

CONCLUSIONS

The foregoing results demonstrate how coordination chemistry principles can be applied to manipulate the enthalpy and entropy of phase transitions relevant to thermal energy storage. In particular, metal−organic PCMs containing compact amide ligands and dense hydrogen bond networks were shown to undergo high-enthalpy, reversible melting transitions, and isostructural series of compounds were used to rationalize trends in phase-change thermodynamics based on both local coordination environments and extended structure (Figure 6). Notably, these metal−organic PCMs achieve volumetric energy densities similar to many metal−salt hydrates despite having significantly lower hydrogen bond densities (Figure S4).

Models of liquid structure revealed that changes to the coordination environment of metal centers during melting dominate entropic differences between isostructural compounds, while enthalpic differences arise mostly from changes to the strength of coordination bonds and intramolecular hydrogen bonds. Across different series of metal−organic PCMs, the density and strength of both hydrogen bonds and coordination bonds are the most important contributors to overall energy density. Future metal−organic PCMs could leverage large changes to the first coordination sphere upon melting, like those observed for Zn-based compounds, to increase both ΔH_{fus} and ΔS_{fus}.

The chemical intuition developed here should be readily extendable to other classes of metal−organic PCMs beyond simple molecular coordination compounds. For example, metal−organic materials with extended networks of coordination bonds present opportunities to leverage dimensionality to further tune the thermophysical properties of PCMs, including those that undergo both solid−liquid and solid−solid phase transitions.[77,78] In addition, the wide parameter space afforded by organic ligand design—coupled with the predictability of directional coordination bonds—should facilitate the exploration of other creative ways of increasing PCM energy density,[79,80] such as by coupling order−disorder transitions to reversible chemical reactions.

ASSOCIATED CONTENT

Supporting Information

The Supporting Information is available free of charge at https://pubs.acs.org/doi/10.1021/jacs.0c08777.

Experimental details, overview of reported metal−salt hydrates for thermal energy storage, DSC cycling data, powder X-ray diffraction data, description of EXAFS

https://dx.doi.org/10.1021/jacs.0c08777
J. Am. Chem. Soc. XXXX, XXX, XXX−XXX

models, and a summary of all structural and thermodynamic data (PDF)
Crystallographic data for all complexes (CIF)

AUTHOR INFORMATION

Corresponding Author

Jarad A. Mason − *Department of Chemistry & Chemical Biology, Harvard University, Cambridge, Massachusetts 02138, United States;* orcid.org/0000-0003-0328-7775; Email: mason@chemistry.harvard.edu

Authors

Ryan D. McGillicuddy − *Department of Chemistry & Chemical Biology, Harvard University, Cambridge, Massachusetts 02138, United States*

Surendra Thapa − *Department of Chemistry & Chemical Biology, Harvard University, Cambridge, Massachusetts 02138, United States*

Malia B. Wenny − *Department of Chemistry & Chemical Biology, Harvard University, Cambridge, Massachusetts 02138, United States*

Miguel I. Gonzalez − *Department of Chemistry & Chemical Biology, Harvard University, Cambridge, Massachusetts 02138, United States*

Complete contact information is available at: https://pubs.acs.org/10.1021/jacs.0c08777

Notes

The authors declare no competing financial interest.

ACKNOWLEDGMENTS

This research was partially supported by the Climate Change Solutions Fund at Harvard University. This research was also partially supported by the Arnold and Mabel Beckman Foundation through a Beckman Young Investigator Award to J.A.M. and a Beckman Postdoctoral Fellowship to M.I.G. Additionally, M.B.W. is supported by the Department of Energy Computational Science Graduate Fellowship under Grant DE-FG02-97ER25308. This work used beamline 12-BM at the Advanced Photon Source, a U.S. Department of Energy (DOE) Office of Science User Facility operated for the DOE Office of Science by Argonne National Laboratory under Contract DE-AC02-06CH11357. We thank Dr. Sungsik Lee for assistance with EXAFS experiments and data analysis. The authors also thank Dr. Shao-Liang Zheng for helpful discussions.

REFERENCES

(1) LLNL Flow Charts: Energy Flow Charts. LLNL-WEB-669625; U.S. Department of Energy, 2020.

(2) (a) Gur, I.; Sawyer, K.; Prasher, R. Searching for a Better Thermal Battery. *Science* **2012**, *335*, 1454−1455. (b) Henry, A.; Prasher, R.; Majumdar, A. Five Thermal Energy Grand Challenges for Decarbonization. *Nat. Energy* **2020**, *5*, 635−637.

(3) de Gracia, A.; Cabeza, L. F. Phase Change Materials and Thermal Energy Storage for Buildings. *Energy and Buildings* **2015**, *103*, 414−419.

(4) Fox, D. B.; Sutter, D.; Tester, J. W. The Thermal Spectrum of Low-Temperature Energy Use in the United States. *Energy Environ. Sci.* **2011**, *4*, 3731−3740.

(5) (a) Snyder, J. G.; Toberer, E. S. Complex Thermoelectric Materials. *Nat. Mater.* **2008**, *7*, 105−114. (b) Zhang, X.; Zhao, L.-D. Thermoelectric Materials: Energy Conversion between Heat and Electricity. *Journal of Materiomics* **2015**, *1*, 92−105.

(6) (a) Jaworski, M.; Bednarczyk, M.; Czachor, M. Experimental Investigation of Thermoelectric Generator (TEG) with PCM Module. *Appl. Therm. Eng.* **2016**, *96*, 527−533. (b) Karthick, K.; Suresh, S.; Joy, G. C.; Dhanuskodi, R. Experimental Investigation of Solar Reversible Power Generation in Thermoelectric Generator (TEG) Using Thermal Energy Storage. *Energy Sustainable Dev.* **2019**, *48*, 107−114.

(7) Ling, Z.; Zhang, Z.; Shi, G.; Fang, X.; Wang, L.; Gao, X.; Fang, Y.; Xu, T.; Wang, S.; Liu, X. Review on Thermal Management Systems Using Phase Change Materials for Electronic Components, Li-Ion Batteries and Photovoltaic Modules. *Renewable Sustainable Energy Rev.* **2014**, *31*, 427−438.

(8) Skach, M.; Arora, M.; Hsu, C.-H.; Li, Q.; Tullsen, D.; Tang, L.; Mars, J. Thermal Time Shifting: Leveraging Phase Change Materials to Reduce Cooling Costs in Warehouse Scale Computers. *ISCA* **2015**, 439.

(9) Hallaj, S. A.; Selman, J. R. A Novel Thermal Management System for Electric Vehicle Batteries Using Phase-Change Material. *J. Electrochem. Soc.* **2000**, *147*, 3231−3236.

(10) Rattner, A. S.; Garimella, S. Energy Harvesting, Reuse and Upgrade to Reduce Primary Energy Usage in the USA. *Energy* **2011**, *36*, 6172.

(11) Roberts, A.; Brooks, R.; Shipway, P. Internal Combustion Engine Cold-Start Efficiency: A Review of the Problem, Causes, and Potential Solutions. *Energy Convers. Manage.* **2014**, *82*, 327−350.

(12) Jankowski, N. R.; McCluskey, F. P. A Review of Phase Change Materials for Vehicle Component Thermal Buffering. *Appl. Energy* **2014**, *113*, 1525−1561.

(13) Stutz, B.; Le Pierres, N.; Kuznik, F.; Johannes, K.; Palomo Del Barrio, E.; Bedecarrats, J.-P.; Gibout, S.; Marty, P.; Zalewski, L.; Soto, J.; Mazet, N.; Olives, R.; Bezian, J.-J.; Minh, D. P. Storage of Thermal Solar Energy. *C. R. Phys.* **2017**, *18*, 401−414.

(14) Kucharski, T. J.; Ferralis, N.; Kolpak, A. M.; Zheng, J. O.; Nocera, D. G.; Grossman, J. C. Templated Assembly of Photoswitches Significantly Increases the Energy-Storage Capacity of Solar Thermal Fuels. *Nat. Chem.* **2014**, *6*, 441−447.

(15) (a) Han, G. G.; Li, H.; Grossman, J. C. Optically-Controlled Long-Term Storage and Release of Thermal Energy in Phase-Change Materials. *Nat. Commun.* **2017**, *8*, 1446. (b) Han, G. G.; Deru, J. H.; Cho, E. N.; Grossman, J. C. Optically-Regulated Thermal Energy Storage in Diverse Organic Phase-Change Materials. *Chem. Commun.* **2018**, *54*, 10722−10725. (c) Gerkman, M. A.; Gibson, R. S. L.; Calbo, J.; Shi, Y.; Fuchter, M. J.; Han, G. G. D. Arylazopyrazoles for Long-Term Thermal Energy Storage and Optically-Triggered Heat Release below 0 °C. *J. Am. Chem. Soc.* **2020**, *142*, 8688−8695.

(16) Matuszek, K.; Vijayaraghavan, R.; Kar, M.; MacFarlane, D. R. Role of Hydrogen Bonding in Phase Change Materials. *Cryst. Growth Des.* **2020**, *20*, 1285−1291.

(17) MacFarlane, D. R.; Tachikawa, N.; Forsyth, M.; Pringle, J. M.; Howlett, P. C.; Elliott, G. D.; Davis, J. H.; Watanabe, M.; Simon, P.; Angell, A. C. Energy Applications of Ionic Liquids. *Energy Environ. Sci.* **2014**, *7*, 232−250.

(18) *Advances in Thermal Energy Storage Systems: Methods and Applications*; Cabeza, L. F., Ed.; Woodhead Publishing Series in Energy: Number 66; Woodhead Publishing: Cambridge, 2015.

(19) Zalba, B.; Marín, J.; Cabeza, L. F.; Mehling, H. Review on Thermal Energy Storage with Phase Change: Materials, Heat Transfer Analysis and Applications. *Appl. Therm. Eng.* **2003**, *23*, 251−283.

(20) Cot-Gores, J.; Castell, A.; Cabeza, L. F. Thermochemical Energy Storage and Conversion: A-State-of-the-Art Review of the Experimental Research under Practical Conditions. *Renewable Sustainable Energy Rev.* **2012**, *16*, 5207−5224.

(21) Pfleger, N.; Bauer, T.; Martin, C.; Eck, M.; Wörner, A. Thermal Energy Storage − Overview and Specific Insight into Nitrate Salts for Sensible and Latent Heat Storage. *Beilstein J. Nanotechnol.* **2015**, *6*, 1487−1497.

(22) Fallahi, A.; Guldentops, G.; Tao, M.; Granados-Focil, S.; Van Dessel, S. Review on Solid-Solid Phase Change Materials for Thermal

Energy Storage: Molecular Structure and Thermal Properties. *Appl. Therm. Eng.* **2017**, *127*, 1427−1441.
(23) Viskanta, R.; Lane, G. A. *Solar Heat Storage*; Lane, G. A., Ed.; CRC Press: Boca Raton, FL, 2018.
(24) Hale, D. V.; Hoover, M. J.; O'Neill, M. J. *Phase Change Materials Handbook*; Technical Report 72N19956 prepared by Lockheed Missiles & Space Company for NASA; Nasa Tech. Rep.: Washington, DC, 1971.
(25) (a) Himran, S.; Suwono, A.; Mansoorith, A. G. Characterization of Alkanes and Paraffin Waxes for Application as Phase Change Energy Storage Medium. *Energy Sources* **1994**, *16*, 117−128. (b) Kahwaji, S.; Johnson, M. B.; Kheirabadi, A. C.; Groulx, D.; White, M. A Comprehensive Study of Properties of Paraffin Phase Change Materials for Solar Thermal Energy Storage and Thermal Management Applications. *Energy* **2018**, *162*, 1169−1182.
(26) Kenisarin, M.; Mahkamov, K. Salt Hydrates as Latent Heat Storage Materials: Thermophysical Properties and Costs. *Sol. Energy Mater. Sol. Cells* **2016**, *145*, 255−286.
(27) (a) Shchukina, E.; Graham, M.; Zheng, Z.; Shchukin, D. Nanoencapsulation of Phase Change Materials for Advanced Thermal Energy Storage Systems. *Chem. Soc. Rev.* **2018**, *47*, 4156−4175. (b) Aftab, W.; Huang, X.; Wu, W.; Liang, Z.; Mahmood, A.; Zou, R. Nanoconfined Phase Change Materials for Thermal Energy Applications. *Energy Environ. Sci.* **2018**, *11*, 1392−1424.
(28) Hyun, D.; Levinson, N. S.; Jeong, U.; Xia, Y. Emerging Applications of Phase-Change Materials (PCMs): Teaching an Old Dog New Tricks. *Angew. Chem., Int. Ed.* **2014**, *53*, 3780−3795.
(29) (a) Mitran, R.; Berger, D.; Munteanu, C.; Matei, C. Evaluation of Different Mesoporous Silica Supports for Energy Storage in Shape-Stabilized Phase Change Materials with Dual Thermal Responses. *J. Phys. Chem. C* **2015**, *119*, 15177−15184. (b) Yang, M.; Luan, Y.; Wang, G.; Qi, Y.; Gao, H.; Ma, Q.; Wu, Z. Introduction of an Organic Acid Phase Changing Material into Metal−Organic Frameworks and the Study of Its Thermal Properties. *J. Mater. Chem. A* **2016**, *4*, 7641−7649.
(30) (a) Microtek Laboratories, Inc. Home Page. https://www.microteklabs.com/ (Accessed Jan 3, 2020). (b) PCM Products Home Page. http://www.pcmproducts.net/ (Accessed Jan 3, 2020). (c) Sutterlin, W. R.; Williams, A. A. Thermal Energy Storage Phase and Temperature Stabilization Change Materials Comprising Triamines and Methods for Making and Using Them. US 2018/0273819 A1, Sep. 27, 2018. (d) Seppälä, A.; Puupponen, S. Cold-Crystallizing Material and Method for Utilizing Cold-Crystallization in Heat Storing. US 2019/0316017 A1, Oct 17, 2019.
(31) Inagaki, T.; Ishida, T. Computational Design of Non-Natural Sugar Alcohols to Increase Thermal Storage Density: Beyond Existing Organic Phase Change Materials. *J. Am. Chem. Soc.* **2016**, *138*, 11810−11819.
(32) Butler, K. T.; Walsh, A.; Cheetham, A. K.; Kieslich, G. Organised Chaos: Entropy in Hybrid Inorganic−Organic Systems and Other Materials. *Chem. Sci.* **2016**, *7*, 6316−6324.
(33) (a) Yaghi, O. M.; O'Keeffe, M.; Ockwig, N. W.; Chae, H. K.; Eddaoudi, M.; Kim, J. Reticular Synthesis and the Design of New Materials. *Nature* **2003**, *423*, 705−714. (b) Kitagawa, S.; Kitaura, R.; Noro, S. Functional Porous Coordination Polymers. *Angew. Chem., Int. Ed.* **2004**, *43*, 2334−2375. (c) Férey, G. Hybrid Porous Solids: Past, Present, Future. *Chem. Soc. Rev.* **2008**, *37*, 191−214. (d) Rao, C.; Cheetham, A.; Thirumurugan, A. Hybrid Inorganic−Organic Materials: A New Family in Condensed Matter Physics. *J. Phys.: Condens. Matter* **2008**, *20*, No. 083202. (e) Aakeröy, C. B.; Champness, N. R.; Janiak, C. Recent Advances in Crystal Engineering. *CrystEngComm* **2010**, *12*, 22−43. (f) Corpinot, M. K.; Bučar, D.-K. A Practical Guide to the Design of Molecular Crystals. *Cryst. Growth Des.* **2019**, *19*, 1426−1453.
(34) Noël, J. A.; Kahwaji, S.; White, M. Molecular Structure and Melting: Implications for Phase Change Materials. *Can. J. Chem.* **2018**, *96*, 722−729.
(35) (a) Telkes, M. In *Solar Materials Science*; Murr, L. E., Ed.; Academic Press: New York, 1980; Chapter 11 pp 377−404. (b) Telkes, M. In *Solar Materials Science*; Murr, L. E., Ed.; Academic Press: New York, 1980; Chapter 12, pp 405−437.
(36) Jenkins, D. H.; Glasser, L. Difference Rule−A New Thermodynamic Principle: Prediction of Standard Thermodynamic Data for Inorganic Solvates. *J. Am. Chem. Soc.* **2004**, *126*, 15809−15817.
(37) Guion, J.; Sauzade, J. D.; Laügt, M. Critical Examination and Experimental Determination of Melting Enthalpies and Entropies of Salt Hydrates. *Thermochim. Acta* **1983**, *67*, 167−179.
(38) Su, W.; Darkwa, J.; Kokogiannakis, G. Review of Solid−Liquid Phase Change Materials and Their Encapsulation Technologies. *Renewable Sustainable Energy Rev.* **2015**, *48*, 373−391.
(39) Duracell Coppertop MN1604 Technical Data Sheet; Duracell: Bethel, CT; No. MN9VCTUS0413.
(40) (a) Ricci, J. S.; Stevens, R. C.; McMullan, R. K.; Klooster, W. T. Structure of Strontium Hydroxide Octahydrate, $Sr(OH)_2{\cdot}8H_2O$, at 20, 100 and 200 K from Neutron Diffraction. *Acta Crystallogr., Sect. B: Struct. Sci.* **2005**, *61*, 381−386. (b) Smith, H. G. The Crystal Structure of Strontium Hydroxide Octahydrate, $Sr(OH)_2{\cdot}8H_2O$. *Acta Crystallogr.* **1953**, *6*, 604−609.
(41) Manohar, H.; Ramaseshan, S. The Crystal Structure of Barium Hydroxide Octahydrate $Ba(OH)_2{\cdot}8H_2O$. *Zeitschrift Für Kristallographie* **1964**, *119*, 357−374.
(42) del Barrio, P. E.; Godin, A.; Duquesne, M.; Daranlot, J.; Jolly, J.; Alshaer, W.; Kouadio, T.; Sommier, A. Characterization of Different Sugar Alcohols as Phase Change Materials for Thermal Energy Storage Applications. *Sol. Energy Mater. Sol. Cells* **2017**, *159*, 560−569.
(43) Solé, A.; Neumann, H.; Niedermaier, S.; Martorell, I.; Schossig, P.; Cabeza, L. F. Stability of Sugar Alcohols as PCM for Thermal Energy Storage. *Sol. Energy Mater. Sol. Cells* **2014**, *126*, 125−134.
(44) Wang, Q.; Wang, J.; Chen, Y.; Zhao, C. Y. Experimental Investigation of Barium Hydroxide Octahydrate as Latent Heat Storage Materials. *Sol. Energy* **2019**, *177*, 99−107.
(45) Hormansdorfer, G. Phase Change Materials and Use Thereof. U.S. Patent 5,085,790, February 4, 1992.
(46) Inagaki, T.; Ishida, T. Computational Analysis of Sugar Alcohols as Phase-Change Material: Insight into the Molecular Mechanism of Thermal Energy Storage. *J. Phys. Chem. C* **2016**, *120*, 7903−7915.
(47) (a) Nardelli, M.; Coghi, L. Complexes of Bivalent Metals with Organic Molecules Containing Oxygen (Formamide, Acetamide, Methylurea). *Ric. Sci.* **1959**, *29*, 134−138. (b) Bailey, R.; Feins, I.; Peterson, T. Nickel(II) Complexes with Substituted Ureas. *Can. J. Chem.* **1969**, *47*, 171−176. (c) Kerridge, D. The Chemistry of Molten Acetamide and Acetamide Complexes. *Chem. Soc. Rev.* **1988**, *17*, 181−227. (d) Keuleers, R.; Papaefstathiou, G.; Raptopoulou, C.; Perlepes, S.; Desseyn, H. O. Comparative Study of the Metal−Ligand Bond Strength in MnII/X/U Complexes (X = Cl, Br, I; U = urea). *J. Mol. Struct.* **2000**, *525*, 173−183. (e) Keuleers, R.; Janssens, J.; Desseyn, H. Thermal Analysis and Vibrational Spectroscopy of Mn(II)−Urea−Halide Complexes: Comparative Study of the Metal−Ligand Bond Strength. *Thermochim. Acta* **2000**, *354*, 125−133. (f) Keuleers, R.; Desseyn, H. O.; Papaefstathiou, G. S.; Drakopoulou, L.; Perlepes, S. P.; Raptopoulou, C. P.; Terzis, A. Hydrogen-Bonded Networks Based on Manganese(II), Nickel(II), Copper(II) and Zinc(II) Complexes of N,N′-Dimethylurea. *Transition Met. Chem. (Dordrecht, Neth.)* **2003**, *28*, 548−557. (g) Papatriantafyllopoulou, C.; Papaefstathiou, G. S.; Terzis, A.; Manessi-Zoupa, E.; Drakopoulou, L.; Perlepes, S. P. Synthesis, X-Ray Structure, and Characterization of a Complex Containing the Hexakis(Urea)Cobalt(II) Cation and Lattice Urea Molecules. *Bioinorg. Chem. Appl.* **2007**, *2007*, 51567.
(48) (a) Diarce, G.; Corro-Martinez, E.; Quant, L.; Campos-Celador, A.; Garcia-Romero, A. The Sodium Nitrate−Urea Binary Mixture as a Phase Change Material for Medium Temperature Thermal Energy Storage. Part I: Determination of the Phase Diagram and Main Thermal Properties. *Sol. Energy Mater. Sol. Cells* **2016**, *157*, 1065−1075. (b) Diarce, G.; Corro-Martínez, E.; Campos-Celador, Á.; García-Romero, A.; Sala, J. M. The Sodium Nitrate−Urea Eutectic

https://dx.doi.org/10.1021/jacs.0c08777
J. Am. Chem. Soc. XXXX, XXX, XXX−XXX

Binary Mixture as a Phase Change Material for Medium Temperature Thermal Energy Storage. Part II: Accelerated Thermal Cycling Test and Water Uptake Behavior of the Material. *Sol. Energy Mater. Sol. Cells* **2016**, *157*, 1076−1083.
(49) Tischer, S.; Börnhorst, M.; Amsler, J.; Schoch, G.; Deutschmann, O. Thermodynamics and Reaction Mechanism of Urea Decomposition. *Phys. Chem. Chem. Phys.* **2019**, *21*, 16785−16797.
(50) (a) Radovanovic, S. B.; Premovic, P. Thermal Behaviour of Cu(II)-Urea Complex. *J. Therm. Anal.* **1992**, *38*, 715−719. (b) Bai, M.; Zhao, S.; Asuha, S. Synthesis and Thermal Decomposition of Cr−Urea Complex. *J. Therm. Anal. Calorim.* **2014**, *115*, 255−258.
(51) Here, volumetric enthalpies were calculated from gravimetric enthalpies by using 25 °C crystal densities calculated from measured unit cell volumes of single crystals and powders. However, we note that the most accurate calculation of volumertic energy storage density would calculate volumetric enthalpies using liquid densities just above the melting point.
(52) Lutz, H. D. Structure and Strength of Hydrogen Bonds in Inorganic Solids. *J. Mol. Struct.* **2003**, *646*, 227−236.
(53) Pike, S. J.; Hutchinson, J. J.; Hunter, C. A. H-Bond Acceptor Parameters for Anions. *J. Am. Chem. Soc.* **2017**, *139*, 6700−6706.
(54) Barrios, A. M.; Lippard, S. J. Decomposition of Alkyl-Substituted Urea Molecules at a Hydroxide-Bridged Dinickel Center. *Inorg. Chem.* **2001**, *40*, 1250−1255.
(55) Irving, H.; Williams, R. J. P. The stability of transition-metal complexes. *J. Chem. Soc.* **1953**, 3192−3210.
(56) (a) Searle, M. S.; Williams, D. H. The Cost of Conformational Order: Entropy Changes in Molecular Associations. *J. Am. Chem. Soc.* **1992**, *114*, 10690−10697. (b) Wei, J. Molecular Symmetry, Rotational Entropy, and Elevated Melting Points. *Ind. Eng. Chem. Res.* **1999**, *38*, 5019−5027.
(57) Nikolić, R.; Ristić, G.; Todorović, M. Binary Eutectics of Acetamide with Inorganic Nitrates: Thermophysical Properties Relevant for Heat Storage. *Sol. Energy Mater. Sol. Cells* **1992**, *28*, 59−69.
(58) Gunasekara, S. N.; Martin, V.; Chiu, J. N. Phase Equilibrium in the Design of Phase Change Materials for Thermal Energy Storage: State-of-the-Art. *Renewable Sustainable Energy Rev.* **2017**, *73*, 558−581.
(59) (a) Pasupathy, A.; Velraj, R. Effect of Double Layer Phase Change Material in Building Roof for Year Round Thermal Management. *Energy and Buildings* **2008**, *40*, 193−203. (b) Fokaides, P. A.; Kylili, A.; Kalogirou, S. A. Phase Change Materials (PCMs) Integrated into Transparent Building Elements: A Review. *Mater. Renew. Sustain. Energy* **2015**, *4*, 6.
(60) Palkina, K. K.; Kuz'mina, N. E.; Orlova, V. T.; Smolentsev, A. Y. Synthesis and Crystal Structure of the Coordination Compounds of Cd(II) and Zn(II) Transition Metal Nitrates with Acetamide. *Zhurnal Neorganicheskoj Khimii* **2002**, *47*, 940−945.
(61) Jones, R. L. Steric Factors Affecting Hydrogen-Bonding between Amide Groups. *Spectrochim. Acta* **1966**, *22*, 1555−1562.
(62) Rozenberg, M.; Loewenschuss, A.; Marcus, Y. An Empirical Correlation between Stretching Vibration Red-shift and Hydrogen Bond Length. *Phys. Chem. Chem. Phys.* **2000**, *2*, 2699−2702.
(63) Johansson, A.; Kollman, P.; Rothenberg, S.; McKelvey, J. Hydrogen Bonding Ability of the Amide Group. *J. Am. Chem. Soc.* **1974**, *96*, 3794−3800.
(64) Hardacre, C. Application of EXAFS to Molten Salts and Ionic Liquid Technology. *Annu. Rev. Mater. Res.* **2005**, *35*, 29−49.
(65) Ohtaki, H.; Radnai, T. Structure and Dynamics of Hydrated Ions. *Chem. Rev.* **1993**, *93*, 1157−1204.
(66) Ravel, B.; Kelly, S. D. The Difficult Chore of Measuring Coordination by EXAFS. *AIP Conf. Proc.* **2006**, *882*, 150−152.
(67) (a) Ozutsumi, K.; Koide, M.; Suzuki, H.; Ishiguro, S. Solvation Structure of Divalent Transition-Metal Ions in N,N-Dimethylformamide and N,N-Dimethylacetamide. *J. Phys. Chem.* **1993**, *97*, 500−502. (b) Inada, Y.; Sugimoto, K.; Ozutsumi, K.; Funahashi, S. Solvation Structures of Manganese(II), Iron(II), Cobalt(II), Nickel(II), Copper(II), Zinc(II), Cadmium(II), and Indium(III) Ions in 1,1,3,3-Tetramethylurea As Studied by EXAFS and Electronic Spectroscopy. Variation of Coordination Number. *Inorg. Chem.* **1994**, *33*, 1875−1880.
(68) Dunitz, J. D. Win Some, Lose Some: Enthalpy-Entropy Compensation in Weak Intermolecular Interactions. *Chem. Biol.* **1995**, *2*, 709−712.
(69) Ford, D. M. Enthalpy−Entropy Compensation Is Not a General Feature of Weak Association. *J. Am. Chem. Soc.* **2005**, *127*, 16167−16170.
(70) (a) Pasquarello, A.; Petri, I.; Salmon, P. S.; Parisel, O.; Car, R.; Tóth, É.; Powell, D. H.; Fischer, H. E.; Helm, L.; Merbach, A. E. First Solvation Shell of the Cu(II) Aqua Ion: Evidence for Fivefold Coordination. *Science* **2001**, *291*, 856−859. (b) Frank, P.; Benfatto, M.; Hedman, B.; Hodgson, K. O. The X-Ray Absorption Spectroscopic Model of the Copper(II) Imidazole Complex Ion in Liquid Aqueous Solution: A Strongly Solvated Square Pyramid. *Inorg. Chem.* **2012**, *51*, 2086−2096. (c) Zitolo, A.; Chillemi, G.; D'Angelo, P. X-Ray Absorption Study of the Solvation Structure of Cu^{2+} in Methanol and Dimethyl Sulfoxide. *Inorg. Chem.* **2012**, *51*, 8827−8833. (d) Frank, P.; Benfatto, M.; Qayyam, M.; Hedman, B.; Hodgson, K. O. A High-Resolution XAS Study of Aqueous Cu(II) in Liquid and Frozen Solutions: Pyramidal, Polymorphic, and Non-Centrosymmetric. *J. Chem. Phys.* **2015**, *142*, No. 084310. (e) Persson, I.; Lundberg, D.; Bajnóczi, É. G.; Klementiev, K.; Just, J.; Clauss, K. G. V. S. EXAFS Study on the Coordination Chemistry of the Solvated Copper(II) Ion in a Series of Oxygen Donor Solvents. *Inorg. Chem.* **2020**, *59*, 9538−9550.
(71) Safari, A.; Saidur, R.; Sulaiman, F. A.; Xu, Y.; Dong, J. A Review on Supercooling of Phase Change Materials in Thermal Energy Storage Systems. *Renewable Sustainable Energy Rev.* **2017**, *70*, 905−919.
(72) Sandnes, B. The Physics and Chemistry of the Heat Pad. *Am. J. Phys.* **2008**, *76*, 546.
(73) Höhlein, S.; König-Haagen, A.; Brüggemann, D. Thermophysical Characterization of $MgCl_2{\cdot}6H_2O$, Xylitol and Erythritol as Phase Change Materials (PCM) for Latent Heat Thermal Energy Storage (LHTES). *Materials* **2017**, *10*, 444.
(74) (a) Lane, G. A. Phase Change Materials for Energy Storage Nucleation to Prevent Supercooling. *Sol. Energy Mater. Sol. Cells* **1992**, *27*, 135−160. (b) Ushak, S.; Gutierrez, A.; Barreneche, C.; Fernandez, A. I.; Grágeda, M.; Cabeza, L. F. Reduction of the Subcooling of Bischofite with the Use of Nucleating Agents. *Sol. Energy Mater. Sol. Cells* **2016**, *157*, 1011−1018.
(75) Shamberger, P. J.; O'Malley, M. J. Heterogeneous Nucleation of Thermal Storage Material $LiNO_3{\cdot}3H_2O$ from Stable Lattice-Matched nucleation catalysts. *Acta Mater.* **2015**, *84*, 265−274.
(76) (a) Porisini, F. C. Salt Hydrates Used for Latent Heat Storage: Corrosion of Metals and Reliability of Thermal Performance. *Sol. Energy* **1988**, *41*, 193−197. (b) Ferrer, G.; Solé, A.; Barreneche, C.; Martorell, I.; Cabeza, L. F. Corrosion of Metal Containers for Use in PCM Energy Storage. *Renewable Energy* **2015**, *76*, 465−469.
(77) Bennett, T. D.; Horike, S. Liquid, Glass and Amorphous Solid States of Coordination Polymers and Metal−Organic Frameworks. *Nat. Rev. Mater.* **2018**, *3*, 431−440.
(78) Bennett, T. D.; Cheetham, A. K. Amorphous Metal−Organic Frameworks. *Acc. Chem. Res.* **2014**, *47*, 1555−1562.
(79) Shamberger, P. J.; Mizuno, Y.; Talapatra, A. A. Mixing and Electronic Entropy Contributions to Thermal Energy Storage in Low Melting Point Alloys. *J. Appl. Phys.* **2017**, *122*, No. 025105.
(80) Zhang, Z. Y.; He, Y.; Wang, Z.; Xu, J.; Xie, M.; Tao, P.; Ji, D.; Moth-Poulsen, K.; Li, T. Photochemical Phase Transitions Enable Coharvesting of Photon Energy and Ambient Heat for Energetic Molecular Solar Thermal Batteries That Upgrade Thermal Energy. *J. Am. Chem. Soc.* **2020**, *142*, 12256−12264.

https://dx.doi.org/10.1021/jacs.0c08777
J. Am. Chem. Soc. XXXX, XXX, XXX−XXX